# Theta phase shift in spike timing and modulation of gamma oscillation: a dynamic code for spatial alternation during fixation in rat hippocampal area CA1

**Muneyoshi Takahashi, Hiroshi Nishida, A. David Redish and Johan Lauwereyns**

*J Neurophysiol* 111:1601-1614, 2014. First published 29 January 2014; doi:10.1152/jn.00395.2013



***Journal of Neurophysiology*** publishes original articles on the function of the nervous system. It is published 12 times a year (monthly) by the American Physiological Society, 9650 Rockville Pike, Bethesda MD 20814-3991.  ISSN: 0022-3077, ESSN: 1522-1598. Visit our website at http://www.the-aps.org/.

*J Neurophysiol* 111: 1601–1614, 2014.
First published January 29, 2014; doi:10.1152/jn.00395.2013.

# Theta phase shift in spike timing and modulation of gamma oscillation: a dynamic code for spatial alternation during fixation in rat hippocampal area CA1

**Muneyoshi Takahashi,[1,2] Hiroshi Nishida,[1] A. David Redish,[3] and Johan Lauwereyns[1,2]**
[1]*Graduate School of Systems Life Sciences, Kyushu University, Fukuoka, Japan;* [2]*Brain Science Institute, Tamagawa University, Tokyo, Japan; and* [3]*Department of Neuroscience, University of Minnesota, Minneapolis, Minnesota*

Submitted 31 May 2013; accepted in final form 23 January 2014

**Takahashi M, Nishida H, Redish AD, Lauwereyns J.** Theta phase shift in spike timing and modulation of gamma oscillation: a dynamic code for spatial alternation during fixation in rat hippocampal area CA1. *J Neurophysiol* 111: 1601–1614, 2014. First published January 29, 2014; doi:10.1152/jn.00395.2013.—Although hippocampus is thought to perform various memory-related functions, little is known about the underlying dynamics of neural activity during a preparatory stage before a spatial choice. Here we focus on neural activity that reflects a memory-based code for spatial alternation, independent of current sensory and motor parameters. We recorded multiple single units and local field potentials in the stratum pyramidale of dorsal hippocampal area CA1 while rats performed a delayed spatial-alternation task. This task includes a 1-s fixation in a nose-poke port between selecting alternating reward sites and so provides time-locked enter-and-leave events. At the single-unit level, we concentrated on neurons that were specifically active during the 1-s fixation period, when the rat was ready and waiting for a cue to pursue the task. These neurons showed selective activity as a function of the alternation sequence. We observed a marked shift in the phase timing of the neuronal spikes relative to the theta oscillation, from the theta peak at the beginning of fixation to the theta trough at the end of fixation. The gamma-band local field potential also changed during the fixation period: the high-gamma power (60–90 Hz) decreased and the low-gamma power (30–45 Hz) increased toward the end. These two gamma components were observed at different phases of the ongoing theta oscillation. Taken together, our data suggest a switch in the type of information processing through the fixation period, from externally cued to internally generated.

theta rhythm; gamma oscillations; spike phase shift; nose-poking paradigm; memory

THE HIPPOCAMPUS IS THOUGHT to perform various memory-related functions, including episode-dependent place recognition, long-term remapping, replay and preplay of potential journeys in an environment (e.g., Davidson et al. 2010; Diba and Buzsáki 2007; Ferbinteanu and Shapiro 2003; Foster and Wilson 2006; Gupta et al. 2010; Johnson and Redish 2007; Karlsson and Frank 2009; Lever et al. 2002; O'Keefe and Nadel 1978; O'Neil et al. 2008; Redish 1999; Sakurai 1994; Wood et al. 2000). To focus specifically on a code for spatial alternation in a delay period before making a choice, we developed a paradigm that includes a crucial fixation period in which the rat is immobile, ready and waiting for the next event (see Fig. 1*A*). Previously, we identified CA1 neurons whose firing during the fixation period was strongly modulated by memory-guided alternation (Takahashi et al. 2009a, 2009b). Here we examine how the alternation coding in this type of neuron relates to the theta rhythm in hippocampal local field potentials (LFPs).

Researchers have emphasized the role of theta (6–12 Hz) in hippocampal information processing (e.g., Bland 2009; Buzsáki 2006; Gupta et al. 2012; Hasselmo 2005; Jezek et al. 2011; Lisman 2005; O'Keefe and Nadel 1978; Vanderwolf 1971), usually focusing on type 1 theta (atropine-resistant) when the rat is actively moving (as opposed to type 2 theta, atropine-sensitive, when the rat is alert, but not moving; Bland 2009; Bland and Oddie 2001; O'Keefe and Nadel 1978; Vanderwolf 1971). The spike timing of CA1 neurons shows a systematic phase relationship, theta phase precession, as the subject moves through a place field (O'Keefe and Recce 1993; Skaggs et al. 1996). Several studies have shown theta phase precession when the rat stays in the same place, running in a running wheel (Harris et al. 2002; Pastalkova et al. 2008), on a treadmill belt (Royer et al. 2012), or on a rotating ball in a virtual reality setup (Harvey et al. 2009). These results suggest that the theta phase precession reflects internally generated processes rather than changes in sensory input.

Other studies have emphasized the importance of hippocampal gamma oscillations (30–90 Hz) and their modulation by theta (e.g., Colgin et al. 2009; Lisman and Redish 2009; Tort et al. 2008). Low-frequency gamma oscillations (30–45 Hz) in CA1 reflect inputs from CA3, while high-frequency gamma oscillations (60–90 Hz) reflect inputs from entorhinal cortex (Bragin et al. 1995; Colgin et al. 2009).

Gamma oscillations occur at different frequencies, depending on running speed (Ahmed and Mehta 2012; Chen et al. 2011; Kemere et al. 2013). However, although low-frequency gamma has been reported during sharp waves in immobility (Carr et al. 2012), it is not known whether both low- and high-frequency gamma oscillations can be observed during an immobile period. Our study goes beyond these various lines of work by examining the relations among individual spikes and oscillations during fixation, when the rat's neural activity reflects a code for spatial alternation in a nose-poke paradigm with a delay.

## MATERIALS AND METHODS

*Subjects.* Four male Wistar/ST rats (Japan SLC) were used, weighing 280–420 g and aged 4–6 mo at the beginning of behavioral training. The rats were food deprived to no less than 80% of their free-feeding body weight during the experiments; water was freely available in the home cage at all times. The rats were housed

Address for reprint requests and other correspondence: M. Takahashi, Brain Science Institute, Tamagawa Univ., 6-1-1 Tamagawa Gakuen, Machida, Tokyo 194-8610, Japan (e-mail: taka@lab.tamagawa.ac.jp).

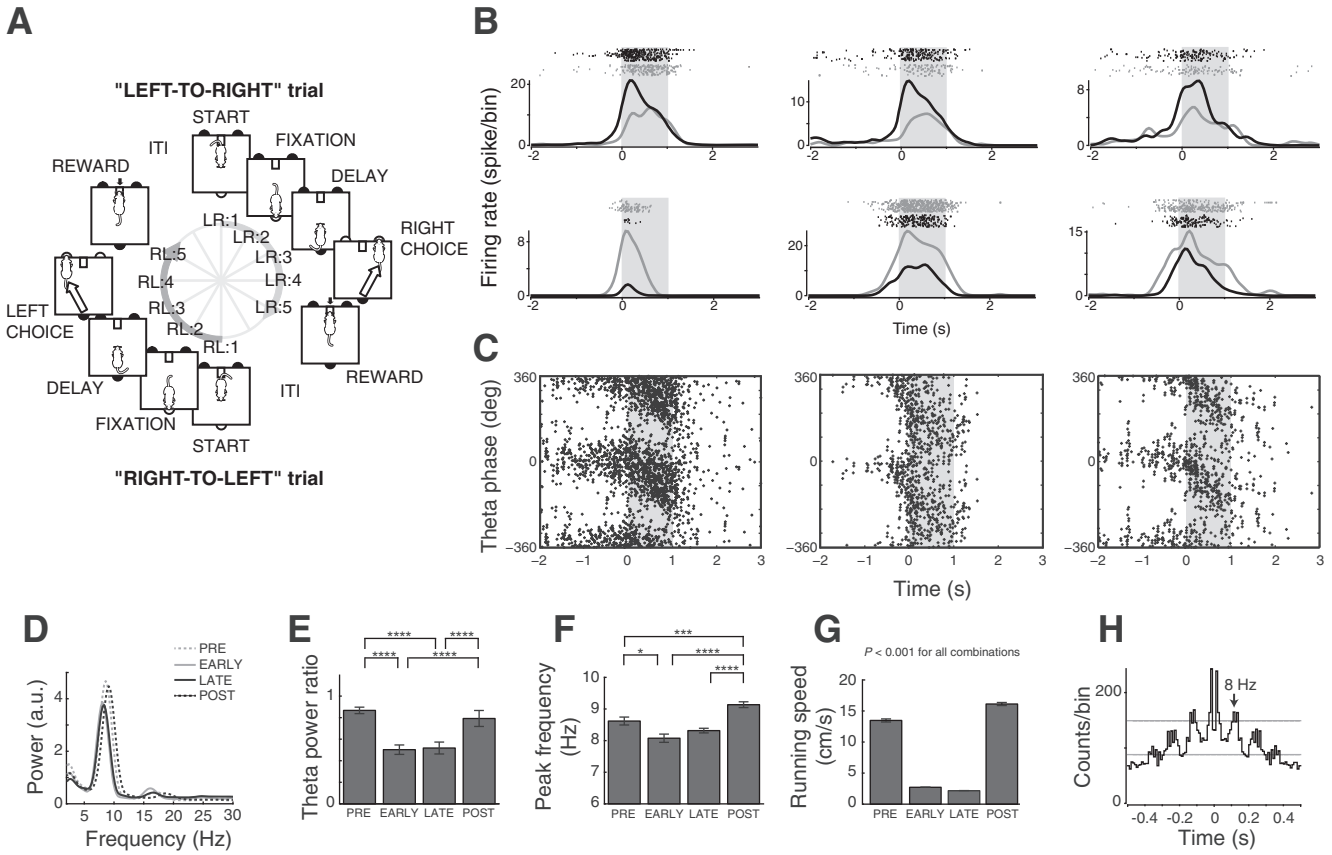


Fig. 1. Memory-guided spatial alternation and fixation-specific hippocampal activity (see also Takahashi et al. 2009a, 2009b). *A*: circular representation of the task events in the nose-poke paradigm. The sequence starting from the *top* represents a LEFT-TO-RIGHT (LR) trial [starting from the *bottom*: RIGHT-TO-LEFT (RL) trial]. ITI, intertrial interval. *B*: raster plots and spike histograms from six examples of the sequence-dependent fixation cell (black lines: RL trials; gray lines: LR trials; fixation period: 0–1 s; bin size: 50 ms). *Top* three panels are RL-preferred type, and the *bottom* three panel are LR-preferred type. *C*: three examples of fixation cells that showed spikes on approach to fixation. Each graph represents a different neuron; each dot represents a spike. This type of cell tended to show phase precession that continued into the fixation period. The shaded zone indicates 1 s of fixation. Phase zero indicates the positive peak of the ongoing theta oscillation. *D*: power spectral density estimates of the hippocampal local field potential (LFP) around fixation (4 periods of 0.5 s; EARLY and LATE represent the first and second half of fixation). au, Arbitrary units. *E*: the mean normalized theta band (6–10 Hz) power rates ($n = 18$ sessions, all data within a session for each period were concatenated and analyzed from power spectral density estimate). *F*: the mean peak frequency in the power spectral density estimates ($n = 18$ sessions, same as *E*). The theta-band power was normalized by the power of the early approaching period, from $-1$ to $-0.5$ s relative to the fixation onset (*$P < 0.05$; ***$P < 0.005$; ****$P < 0.001$). *G*: the mean locomotion (running speed) around fixation ($n = 1{,}181$ trials). *H*: autocorrelogram for the example neuron in the *top left* section of *B*, indicating a significant theta-band rhythmic firing (peak at 8 Hz; bin width: 10 ms; two gray lines indicate the 99.5% statistical confidence limits).

individually with a 14:10-h light-dark cycle. All behavioral training and neural recording sessions were conducted during the light period from 7:00 AM to 9:00 PM. All procedures were in accordance with the National Institutes of Health guidelines for animal care and were approved by the Tamagawa University Animal Care and Use Committee.

*Apparatus.* Behavioral training and neuronal recording were carried out in an experimental chamber constructed of Plexiglas (40 × 40 × 40 cm; Takahashi et al. 2009a, 2009b). The experimental chamber was fitted within a sound-attenuating box and illuminated by a 15-W light bulb, serving as a house light. Two peripheral nose-poke holes were located on the front wall of the chamber: one at 10 cm to the right and one at 10 cm to the left of the center. The third nose-poke hole was located at the center of the rear wall. Each nose-poke hole was 2 cm in diameter, 2 cm deep, and located 4 cm above the floor. Light-emitting diodes at the rear of each hole were used as visual cues. Horizontal infrared photo-beam detectors in the hole were used to record the nose-poking responses. A food dispenser (PD-25D; O'Hara) delivered 25-mg food pellets (O'Hara) to a receptacle that was located 4 cm above the floor and at the middle of the front wall. A 0.5-s buzzer sound was presented at the time of reward delivery. A charged-coupled device camera was mounted on the ceiling of the sound-attenuating box for video tracking of the animal's position with a sampling rate of 60 Hz (Neuralynx). All events were controlled by customized software developed with Microsoft Visual C++ 6.0 on a Windows-based personal computer.

*Behavioral task.* The memory-guided spatial alternation task involved the following sequence of events (Fig. 1*A*; Takahashi et al. 2009a, 2009b). A trial started when only the center hole light was illuminated. The rat was then required to make a nose-poke response, which had to be sustained for 1 s in the central hole (i.e., the fixation period). After 1-s sustained fixation, the central light was extinguished, and after a delay of 1.5 s, the right and left lights were simultaneously illuminated on the front wall. The rat had to alternate between choosing the right and left hole on a trial-by-trial basis and was rewarded with a food pellet for each correct choice. If the rat made an erroneous choice, no reward was given, and the same trial was repeated (i.e., a correction trial). The correct direction for the first trial in each session was determined pseudorandomly. The intertrial interval was 10 s. Training and recording sessions continued for a maximum of 200 correct trials, not including correction trials, or until 60 min had elapsed. The training was completed when the rat was able to perform three consecutive sessions with an accurate choice rate of more than 80% and a total of more than 100 correct trials per session.

*Electrodes and surgery.* After the completion of behavioral training, a 14-tetrode microdrive (Neuro-hyperdrive; David Kopf Instruments) was implanted in each rat, directed toward the dorsal hippocampal CA1 subfield (3.6 mm posterior to the bregma and 2.2 mm right-lateral relative to the midline) in accordance with the brain atlas by Paxinos and Watson (2004). Tetrodes were constructed from polyimide-insulated 12.7-$\mu$m nichrome wire (Rediohm-800; Kenthal) and gold plated to reduce the impedance to the 250- to 300-k$\Omega$ range (measured at 1 kHz; BAK Electronics IMP-1). Details of the surgical procedure were as presented previously (Takahashi et al. 2009a, 2009b). Briefly, rats were anesthetized with a mixture of ketamine (100 mg/kg ip) and xylazine (7 mg/kg ip). Additional intramuscular injections of ketamine were given to maintain anesthesia. The hyperdrive was then secured in place with dental acrylic, supported by eight anchor screws and a ground screw. Immediately after surgery, all electrodes were advanced about 1 mm. Rats were allowed more than 5 days to recover from surgery before the behavioral experiments were resumed.

*Data collection.* The neuronal data and the behavioral events were recorded using the Cheetah 160 Data Acquisition System (Neuralynx). For spike recording, tetrode channels were band-pass filtered (600–6,000 Hz), differentially amplified ($\times$2,000–5,000), and digitized at 32 kHz. When the voltage on any of the four channels of a single tetrode exceeded a threshold set by the experimenter, a 1-ms window of the spike waveform on each of the four channels on the tetrode was recorded to disk and time-stamped with microsecond resolution. For LFP recording, the most prominent channel of each tetrode was picked out, band-pass filtered (1–475 Hz), differentially amplified ($\times$2,000), digitized at 2 kHz, and stored to disk.

Each tetrode was slowly advanced toward the hippocampus from 80 to 320 $\mu$m/day while monitoring the unit activity when the animal was lying on a small table (30 cm in diameter, 1 m above the floor), either asleep or quietly resting. The reference electrodes were positioned in the corpus callosum or silent white matter (the absence of theta oscillations was visually confirmed during the initial adjusting of the reference electrodes). On the way to the pyramidal cell layer of CA1, we observed low-frequency sharp waves with high-frequency ripples (Csicsvari et al. 1999; Ylinen et al. 1995). At this point, we gradually advanced the tetrodes until we detected multiple single units. The animal was then returned to its home cage. If the neuronal activity was still present after 2 h, it was judged to be stable and suitable for recording (Sakurai 1994, 1996).

After all the recording sessions were completed, we marked the location of each tetrode by passing a small amount of current through one channel for each tetrode (30 $\mu$A for 5 s) to obtain histological evidence of the recording site.

*Data analysis: spike sorting.* Our database included neurons from which activity was recorded during sessions of more than 100 trials at 80% accuracy. Putative single neurons were isolated using MClust 3.5 (Redish et al.; http://redishlab.neuroscience.umn.edu/MClust/MClust.html) after automatic preclustering using KlustaKwik 1.7 (Harris; http://klustakwik.sourceforge.net/). The first to third principal components and the energy (i.e., sum of square values for each sampling point of the 1-ms waveform; Schmitzer-Torbert and Redish 2004) were used as the waveform features for spike sorting. To judge whether the calculated cluster actually consisted of only one neuron, we performed autocorrelation analysis for each cluster at 1-ms bin size to check the refractory period. If the autocorrelogram showed no spikes less than 2 ms, we regarded it a well-separated cluster and used it for further analyses.

A neuron was identified as a pyramidal cell if its waveform had a width of more than 270 $\mu$s (Smith and Mizumori 2006), if it showed bimodal interspike interval distribution that reflected complex spike bursting (Bower et al. 2005), and if it had a low mean firing rate over the entire recording session (less than 2 Hz).

*Data analysis: unit categorization.* As a first screening, to characterize the firing trends of recorded CA1 neurons, we defined three subperiods around the fixation period: 1 s before the fixation onset; 1 s during the fixation period; and 1 s after the fixation cue offset. Excluded from analyses (unless mentioned explicitly, for the analysis of error trials) were data from erroneous-choice trials, correction trials, and trials in which the rat made premature fixation breaks or nose-poking responses before the trial start. For each subperiod, a Wilcoxon signed-rank test was conducted (with alpha level at 0.05) to check for a significant increase of the firing rate against the average firing rate of each trial.

For subperiods in which we detected a significant increase, we tested whether the firing trend showed sequence dependency by conducting a Mann-Whitney *U*-test on RIGHT-TO-LEFT vs. LEFT-TO-RIGHT trials. Neurons that showed the same type of sequence dependency throughout all significant subperiods were categorized as "simple," whereas the other types were categorized as "complex" (e.g., with a switch in sequence preference, or with no sequence dependency in one of the significant subperiods).

Next, to focus more specifically on fixation activity, we considered a neuron's spiking activity to be fixation specific (and the neuron was labeled "a fixation unit") if the firing rate during fixation was higher than that during the task periods right before and right after fixation, that is, both of the following indexes, $I_{pre}$ and $I_{post}$, produced values $< 0.5$:

$$I_{pre} = \frac{fr(Pre)}{fr(Pre) + fr(Fix)}$$

and

$$I_{post} = \frac{fr(Post)}{fr(Post) + fr(Fix)}$$

where $fr(X)$ denotes the firing rate during period $X$, and *Pre, Fix*, and *Post* denote the prefixation period, the fixation period, and the postfixation period (1 s for each), respectively.

*Data analysis: LFP preprocessing.* Before all LFP analyses, the direct current offsets and slowly changing components were removed from the LFP data by applying the *locdetrend* function in the Chronux 2.00 toolbox (http://www.chronux.org) (Bokil et al. 2010; Mitra and Bokil 2008), which subtracts the linear regression line fit within a 1-s window.

*Data analysis: spike timing analysis.* To obtain a theta phase angle for each spike, LFPs recorded from the same tetrode were filtered offline to extract their theta-band rhythms (6–10 Hz). We obtained the real and imaginary part of the analytical representation of the LFP signal using Hilbert transform [$R(t)$ and $I(t)$, respectively]. The instantaneous phase angle was then calculated as $\tan^{-1} I(t)/R(t)$. Data from all sequence-dependent fixation units that showed more than 100 spikes in total during the fixation periods in a single recording session were merged. We created time-to-phase color plots of the spike timing to elucidate the general trends in the spiking activity of CA1 sequence-dependent fixation units in terms of theta phase-based modulation during the fixation period.

*Data analysis: linearity test for spike phase shift.* To evaluate the linearity of the spike phase shift during the fixation period, we estimated linear regressions for the population and for individual trial data based on a method for quantifying circular-linear associations proposed by Kempter et al. (2012). We estimated a value $\hat{a}$ which maximizes the mean resultant length $R$:

$$R = \sqrt{\left[\frac{1}{n}\sum_{j=1}^{n}\cos(\phi_j - 2\pi a t_j)\right]^2 + \left[\frac{1}{n}\sum_{j=1}^{n}\sin(\phi_j - 2\pi a t_j)\right]^2}$$

$$\hat{a} = \arg\max_a R$$

where $\phi_j$ denotes the measured phase angles ($j = 1$ to $n$), and $t_j$ denotes the corresponding value which has a linear relationship to $\phi_j$ (i.e., the time stamp of the spike). However, since this estimated slope

$\hat{a}$ cannot be determined uniquely, we needed to set an adequate range. Here, we employed a Monte Carlo method using random values in the range from −1 to 0. We then introduced the steepest descend method to estimate the value $\hat{a}$ using initially the value $a$ that produces the biggest $R$. The estimated circular-linear (i.e., phase-time) regression line then was described as follows:

$$\widetilde{\phi_j} = 2\pi a t_j + \hat{\phi}_0$$

$$\hat{\phi}_0 = \arctan * \frac{\sum_j \sin(\phi_j - 2\pi\hat{a}t_j)}{\sum_j \cos(\phi_j - 2\pi\hat{a}t_j)}$$

where $\widetilde{\phi_j}$ denotes a predicted angle and $\hat{\phi}_0$ denotes the estimated phase-offset. The function arctan* is the quadrant-specific inverse of the tangent.

*Data analysis: gamma-band oscillation analysis.* To visualize how the strength of gamma-band oscillation changed during fixation, we calculated the spectrograms as follows. We used LFP data obtained from the same tetrodes that recorded the spiking activity in the pyramidal cell layer of hippocampal CA1 subfield. The target period for this analysis was 2 s, lasting from 0.5 before to 0.5 s after fixation. The window width was set at 300 ms and moved with 30-ms steps. The power of the population trend was normalized by dividing the total power of the 4-s (wider) period, including the target period (i.e., 1.5 before to 1.5 s after fixation), at every 0.5 Hz of the frequency band. We also conducted the power spectral density (PSD) analysis for high (60–90 Hz) and low (30–45 Hz) gamma bands for four 0.5-s periods around fixation: PRE, EARLY, LATE, and POST (where EARLY and LATE represent the first and second half of fixation). The PSD estimate for each period was normalized by that of a baseline period for each gamma band, which was another 0.5-s before the PRE (i.e., −1.0 to 0.5 s). These power ratios were compared statistically by one-way repeated-measures ANOVA. This was done to compare the power of gamma oscillation between mobile and immobile periods, and within the immobile period (comparing between the first and second halves).

*Data analysis: modulation of gamma oscillation by theta.* To investigate the cross-frequency coupling between theta and gamma oscillations in hippocampal CA1 during the fixation period, we calculated the time-frequency plots of the mean normalized power, time-locked to the theta trough, as described by Canolty and colleagues (2006) (see also Tort et al. 2008). Because the theta oscillation during fixation was relatively unstable in terms of its instantaneous frequency and amplitude compared with the mobile period, we also computed the theta phase-based mean normalized gamma power, producing a phase-frequency plot. In this method, the dynamics of theta-based comodulation are drawn not on the basis of time course, but on the basis of the theta phase angle.

First, the raw LFP signal data were filtered to the theta range (6–12 Hz, 1-Hz step) and the gamma range (30–90 Hz, 2 Hz step), denoted as follows:

$$x_{i,\theta}(t) = filt_\theta\left[x_{i,r}(t)\right]$$

and

$$x_{i,\gamma}(t) = filt_\gamma\left[x_{i,r}(t)\right]$$

where $x$ stands for the (filtered) LFP signal; $t$ means time; and $r$, $\theta$, $\gamma$, and $i$ are the indexes for the raw signal, the theta band data, the gamma data, and the trial number, respectively. The function $filt(x)$ indicates a band-pass filter. Next, we calculated the $z$-scored $x_{i,\gamma}(t)$ by the total session data, and calculated the instantaneous phase angle and instantaneous amplitude (envelope) using Hilbert transform of the LFP signal $x$, $H(x)$, applied to all LFP data:

$$\phi_{i,\theta} = \tan^{-1}\left\{H\left[x_{i,\theta}(t)\right] / x_{i,\theta}(t)\right\}$$

and

$$a_{i,\gamma} = \sqrt{\left[\tilde{x}_{i,\gamma}(t)\right]^2 + \left\{H\left[\tilde{x}_{i,\gamma}(t)\right]\right\}^2}$$

where $\phi$ denotes the instantaneous phase angle, $a$ denotes the instantaneous amplitude, and $\tilde{x}$ denotes the $z$-scored $x$. Then we defined the normalized instantaneous gamma power $P$ corresponding to the instantaneous phase angle at the time $t$ as follows:

$$P_{i,\gamma}(\phi_{i,\theta}) = \left\{\phi_{i,\theta}(t), \left[a_{i,\gamma}(t)\right]^2\right\}$$

Finally, all trial data were realigned by the theta trough nearest to the fixation onset, and the normalized instantaneous gamma power data were averaged across the trials:

$$P_\gamma(\phi_\theta) = \frac{1}{N}\sum_{i=1}^{N} P_{i,\gamma}(\phi_{i,\theta})$$

where $N$ is the total number of trials.

To determine whether there was interaction between the theta and gamma ranges, we quantified the phase-to-amplitude modulation by the Modulation Index (Tort et al. 2008, 2009, 2010), based on a normalized entropy measure. This allowed us to examine the cross-frequency coupling between the two frequency ranges of interest. Phase-to-amplitude comodulogram plots were constructed by applying this measure to multiple-frequency band pairs made up of "phase frequency" (i.e., theta band: 6–12 Hz; 1-Hz steps with 2-Hz bandwidths) and "amplitude frequency" (i.e., gamma band: 30–90 Hz; 2-Hz steps with 4-Hz bandwidths), stepped through two theta cycles around the target event of interest. We excluded monotonic linear trends by applying the *locdetrend* function in Chronux 2.00 toolbox before computing the Modulation Index. To assess the statistical significance of the Modulation Index values, we worked with a distribution of 200 surrogate Modulation Index values achieved by applying the Modulation Index measure to a trial-shuffled composite time series, similar to the procedure applied by Tort et al. (2008). Assuming a normal distribution for the surrogate Modulation Index values, we set the threshold for significance at $P < 0.01$ in the current study.

*Data analysis: erroneous-trial fixation data analysis.* The database for the erroneous fixation trials was constructed solely on the basis of first-time erroneous fixation breaks in any trial (i.e., excluding any later fixation breaks in the same trial).

To investigate the relationship between the spike timing and the ongoing theta band oscillation in LFP during the erroneous fixation trials, we divided the database of the erroneous fixation trials into three groups on the basis of the duration of fixation: short fixation (with a fixation duration of 0–0.33 s), medium fixation (0.34–0.66 s), and long fixation (0.67–1 s). We created time-to-phase color plots of the spike timing for each of these three groups of erroneous-fixation trials.

To examine the relationship between the gamma-band oscillation and the timing of the premature fixation break in erroneous fixation trials, we conducted a power spectrogram analysis (following the procedures described in the previous section) for the three groups of erroneous-fixation trials.

## RESULTS

We recorded a total of 248 putative CA1 pyramidal neurons from four rats during 18 recording sessions, performing an average of 112.4 correct trials per session (with a standard deviation, SD, of 34.9) at a correct choice rate of 88.9% (SD 6.0). The mean width of the waveforms recorded from these neurons was 347.7 $\mu$s (SD 42.6); the mean firing rate was 0.75 Hz (SD 0.55).

Table 1 presents an overview of the screening of the neurons, categorized as a function of their activities during three 1-s periods: before, during, and after fixation. Seventy-six units

Table 1. *Categorization of CA1 neurons as a function of consistency of the alternation coding in the spike rates around the fixation period*

| | Simple | Complex | Nonselective | Total |
|---|---|---|---|---|
| Fixation cell | | | | (76) |
| During only | 7 | n/a | 7 | 14 |
| During and Before | 6 | 14 | 18 | 38 |
| During and After | 1 | 1 | 0 | 2 |
| During, Before, and After | 0 | 17 | 5 | 22 |
| Others | | | | (172) |
| Before only | 8 | n/a | 15 | 23 |
| After only | 10 | n/a | 5 | 15 |
| Before and After | 1 | 6 | 3 | 10 |
| Not active | | | | 124 |

n/a, Not applicable.

showed significant firing during fixation. Sixty-two of these units (82.6%) combined the fixation activity with significant activity in other periods, particularly in the approach to fixation (60 units; 79.0%). More cells showed combined approach-to-fixation and fixation activity (38 cells) than leaving-from-fixation activity and fixation activity (2 cells); a $\chi^2$ test showed this difference to be significant ($\chi^2 = 32.4$, degrees of freedom = 1, $P < 0.001$).

Several examples of fixation cells are shown in Fig. 1*B*. Cells that increased their firing on approach to fixation tended to show phase precession that continued into fixation (Fig. 1*C*). There were not enough cells to examine phase shift trends postfixation. With respect to the type of alternation coding, 46 of the 76 fixation cells (60.5%) showed sequence dependency (i.e., a firing preference for RIGHT-TO-LEFT vs. LEFT-TO-RIGHT trials) in at least one of the periods; the remaining 30 cells (39.4%) were entirely nonselective. Thirty-two units (42.1%) showed "complex" preference patterns such that sequence dependency occurred in one period but not another, or showed a switch in preference for RIGHT-TO-LEFT vs. LEFT-TO-RIGHT trials. None of the neurons showed a "simple" preference pattern across all three periods.

Next, we focused more specifically on the fixation activity by selecting neurons that showed more dominant activity in the fixation period relative to the periods before and after the fixation, using $I_{pre}$ and $I_{post}$ indexes (see MATERIALS AND METHODS). We obtained 49 units that showed fixation-specific firing by this criterion. Twenty-eight of these units (57.1%) exhibited sequence-dependent activity. Of the sequence-dependent fixation units, 13 preferred RIGHT-TO-LEFT trials; the other 15 preferred LEFT-TO-RIGHT trials (see also Takahashi et al. 2009a, 2009b).

*Spike timing analysis relative to theta oscillation.* The electrodes were located in the CA1 pyramidal cell layer, as confirmed by the presence of sharp wave-ripples and complex spike bursts during both slow-wave sleep and quiet awake periods. For the LFP analyses, we selected the most prominent tetrode wire from which fixation cells were obtained for each recording session. The database was constructed from a total of 31 tetrodes in 18 recording sessions. The number of sessions per animal and the number of trials for each of those sessions are shown in Table 2. LFP data during the fixation period was extracted from the selected tetrodes for each recording session, and the power spectrum was calculated using all session data (Fig. 1*D*). Theta-band oscillation in LFP was observed throughout fixation. This evidence suggests that the subjects were fully alert and not resting during the 1 s of fixation. We divided the fixation period into first and second halves (EARLY and LATE) and examined the difference in theta power (6 to 10 Hz) normalized by the power of the early approaching period (−1 to −0.5 s before the fixation onset). We also examined the peak frequency compared with the 0.5-s mobile periods before (PRE) and after (POST) fixation. The theta power and the peak frequency were computed from each of 18 recording sessions. To check the locomotion level during the fixation period, the running speed was also compared among the four periods described above ($n = 1{,}181$ trials from 18 sessions).

A one-way repeated-measures ANOVA showed statistical differences among the four periods for both theta power [$F(3,51) = 28.6$, mean square error (MSe) = 0.022, $P < 0.001$] peak frequency [$F(3,51) = 23.8$, MSe = 0.158, $P < 0.001$], and running speed [$F(3,3540) = 1{,}985.1$, MSe = 31.05, $P < 0.001$]. Post hoc pair-wise comparisons with Bonferroni correction for the theta power showed significant differences between PRE vs. EARLY ($P < 0.001$), PRE vs. LATE ($P < 0.001$), EARLY vs. POST ($P < 0.001$), and LATE vs. POST ($P < 0.001$) (Fig. 1*E*). For the peak frequency, there were significant differences between PRE vs. EARLY ($P < 0.05$), PRE vs. POST ($P < 0.005$), EARLY vs. POST ($P < 0.001$), and LATE vs. POST ($P < 0.001$) (Fig. 1*F*). For the running speed, there were significant differences between all possible combinations ($P < 0.001$) (Fig. 1*G*).

With respect to the spiking of the fixation cells, we also observed modulation by the theta rhythm during the fixation period (an example of an autocorrelogram is shown in Fig. 1*H*). Of the 28 sequence-dependent fixation units, 24 produced more than 100 spikes in total during the fixation periods in a single task session. Therefore, we decided to examine the relationship between spike timing and the ongoing theta band oscillation in the LFP.

We drew colored-map histograms of spike timing vs. the spiking phase angle for each neuron during a single recording session. The bin size was 50 ms for the time axis, and 10° for the phase angle axis. To improve the visibility of the phase shift, we applied a Gaussian filter (5 × 5 bins, 4 SD). Several examples are shown in Fig. 2*A*. The spikes mainly occurred at the positive peaks of the theta cycles at the beginning of fixation, but shifted to the negative trough at the end of fixation. We noted that this shift in spike timing was stronger for trials with the preferred sequence. Next, we calculated population histograms (Fig. 2*B*) and graphed the mean values for each 0.1-s bin (Fig. 2*C*). The population data clearly showed the phase shift from positive peak to negative trough only in the preferred-sequence trials. We also applied this analysis with a subsampling version in which the same number of spikes were pseudorandomly selected from each 0.1-s bin

Table 2. *A summary of database*

| | *Rat 1* | *Rat 2* | *Rat 3* | *Rat 4* | Total |
|---|---|---|---|---|---|
| Sessions | 6 | 3 | 5 | 4 | 18 |
| Trials | 317 | 335 | 240 | 289 | 1,181 |
| Tetrodes with fixation cells | 11 | 6 | 8 | 6 | 31 |
| Fixation cells | 24 | 15 | 28 | 9 | 76 |

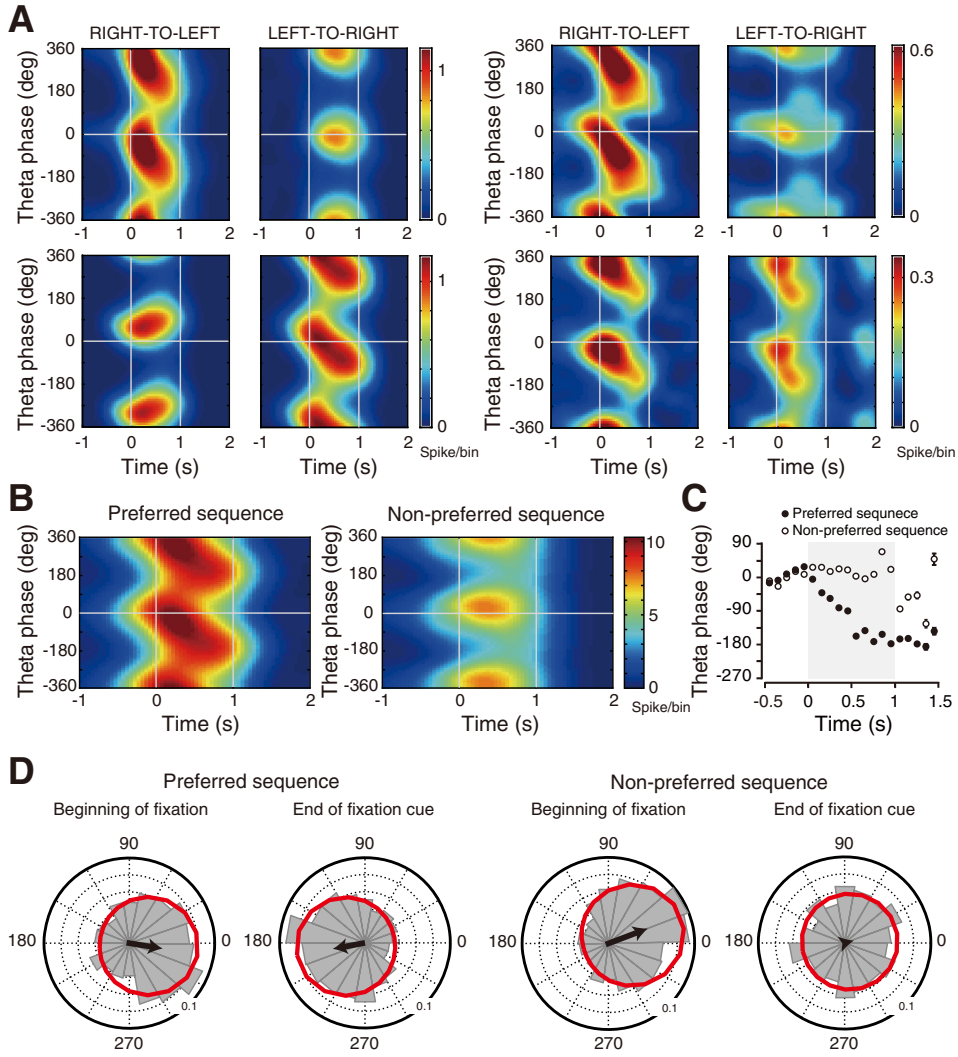


Fig. 2. The theta phase shift in spike timing during the fixation period. *A*: activity from four example neurons, shown on a colored map of spike timing vs. spiking phase angle. The phase shifts of each neuron are shown separately for the RL and LR sequences (bin width: 10°, 50 ms; fixation period: 0–1 s). Zero degrees corresponds to the positive peak of the ongoing theta oscillation. The preferred sequence for each example neuron is LR for the *left bottom* one, and RL for the others. *B*: colored maps of the population data in the same format as that for *A* (24 neurons). *C*: the mean spiking phase angles for each 0.1-s bin. Error bars indicate SEM. *D*: angle histogram plots, shown separately for the preferred vs. nonpreferred sequence (time window for "Beginning of fixation" = 0–0.15 s after fixation onset; for "End of fixation cue" = 0.85–1 s after fixation onset). The radial axis indicates the spiking probability for the corresponding direction (bin width: 18°). The arrow in each plot indicates the mean firing profile; the red lines indicate the estimated probability distribution fitted to the von Mises distribution (circular normal distribution).

and confirmed that this trend was robust for the number of spikes (data not shown).

To examine this phase-shift statistically, we tested the bias in spike phase angle from 0 to 0.15 s after fixation onset and for the last 0.15 s before the fixation cue offset (Fig. 2*D*). We performed V tests for nonuniformity of circular data with a specified mean direction (Zar 2007). For the spike data around the fixation onset in preferred-sequence trials, the spike timings were significantly biased to the positive peak (0°) of the theta cycle ($P < 0.001$; $n = 1{,}028$ spikes). Conversely, in these trials there was a significant bias to the negative trough of the theta cycle (180°) around the offset of the fixation cue ($P < 0.001$; $n = 768$ spikes). In the nonpreferred-sequence trials, no significant shift was observed ($n = 532$ spikes for the fixation onset, and 466 for the offset of the fixation cue).

We also examined the phase-time regression line for the fixation period on a trial-by-trial basis. For this analysis, we used all preferred-sequence trials with more than 10 spikes during fixation, recorded from sequence-dependent fixation cells that showed a total of more than 100 spikes during fixation ($n = 24$). The population phase-time plot is shown in Fig. 3*A*; in this plot, the spike phase shift appears to occur linearly. Figure 3*B* shows the distribution of linearity estimates for all trials; Fig. 3*C* focuses on individual examples. High $R$ values indicate that the spike phase shift occurred linearly within a single trial; the slope $a$ indicates the change rate of the spiking phase angles. The population slope of the estimated phase-time regression line was −0.5376 (Fig. 3*A*), whereas the mean obtained from the slopes estimated for individual trials was −0.4156 ($n = 364$). Only 19 trials (5.2%) occurred within the range of the confidence limits of mean slope data. This result implies that the shift for most of the individual trials did not match the linear regression obtained for the population. The vast majority of trials showed spike phase shifts with poor fits for linearity. Thus, at the single trial level, the spike phase shifts did not occur gradually in a linear fashion, indicating that the trend at the population level only emerges through averaging. Instead, the phase shifts in individual trials often occurred abruptly (as in the top trial in Fig. 3*C*) or went through an unstable, noisy phase, with spikes jumping back and forth between peak and trough (as in the bottom three trials in Fig. 3*C*).

*Gamma-band analysis.* To investigate the gamma-band power during fixation, we calculated the normalized spectrogram during fixation ($n = 1{,}181$ trials; Fig. 4*A*). The period from $t = 0$–1 s is the fixation period. High-gamma power decreased, whereas low-gamma power increased across the fixation period. Focusing on the LFP traces of each frequency

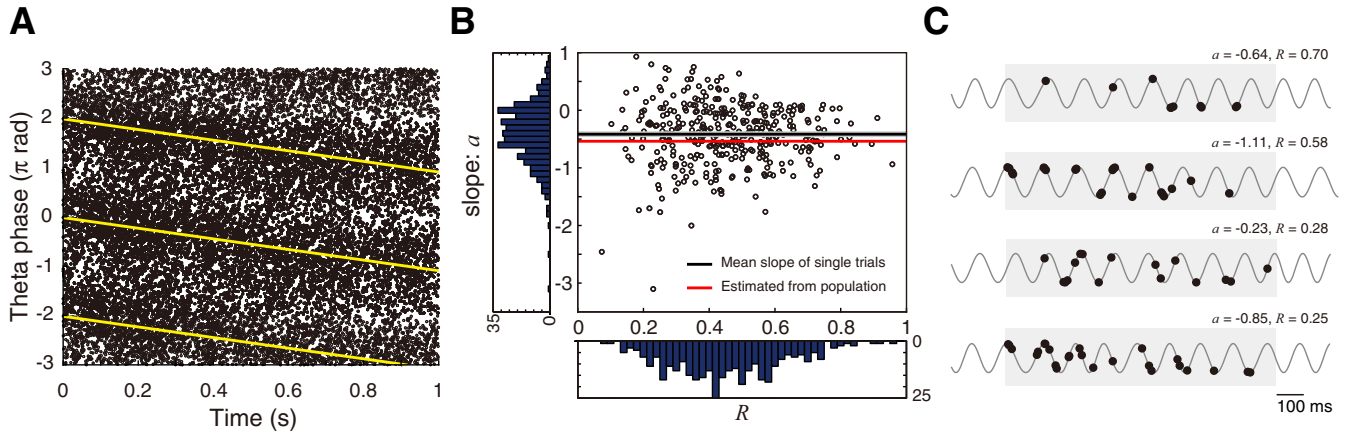


Fig. 3. Linearity estimates for the spike phase shift in the preferred sequence trials. *A*: population data of the spike timing as a function of the theta phase. Each dot indicates a spike; time zero indicates fixation onset. The yellow lines are regression lines calculated using Monte Carlo and the steepest descent methods. *B*: data distribution for the relationship between the slope of the estimated regression line ($a$) and the linearity index ($R$) for individual trials that contained more than 10 spikes during the fixation period. The black horizontal line indicates the mean slope on the basis of all slopes from individual trial data (i.e., the mean of all slopes). The gray area around the black horizontal line represents the confidence interval. The red line shows the estimated slope for the population data (i.e., the slope of the population). The histogram on the vertical axis shows the distribution of the slope parameter $a$ (bin width = 0.1); the horizontal histogram shows the distribution of $R$ (bin width = 0.02). *C*: individual trial examples of spike timing relative to the ongoing theta oscillation. The four examples are selected to illustrate the variety of linearity indexes ($R$). The shaded area indicates the fixation period. The amplitude of the theta-band LFP was normalized to facilitate inspection of the phase relationship.

band (Fig. 4*B*), the high- and low-gamma components appeared to be phase-locked to the ongoing theta oscillation, albeit in different phases.

To quantify the gamma-band power changes, we employed PSD analyses (Fig. 4*C*). For the gamma-band LFP analyses, the gamma-band database was constructed in the same way as for the theta-band database, described above. We divided the fixation period into first and second halves (EARLY and LATE) and examined the difference in the power of low-gamma (30–45 Hz) and high-gamma (60–90 Hz), normalized by the power of the early approaching period (−1 to −0.5 s from the fixation onset). The data were compared with the 0.5-s mobile periods before (PRE) and after (POST) the fixation period.

With respect to the high-gamma data, a one-way repeated-measures ANOVA showed a significant main effect for the four periods [$F(3,51) = 10.5$, MSe = 0.025, $P < 0.001$]. Post hoc pairwise comparisons with Bonferroni correction indicated significant differences between PRE vs. LATE ($P < 0.001$), EARLY vs. LATE ($P < 0.001$), and LATE vs. POST ($P < 0.05$).

The low-gamma data also showed a significant main effect with the four periods in a one-way repeated-measures ANOVA [$F(3,51) = 33.3$, MSe = 0.032, $P < 0.001$]. Post hoc pairwise comparisons with Bonferroni correction obtained significant differences between PRE vs. POST ($P < 0.05$), EARLY vs. LATE ($P < 0.01$), EARLY vs. POST ($P < 0.05$), and all other possible combinations ($P < 0.001$).

The most striking difference was that high-gamma power proved to be stronger at the beginning of fixation (EARLY) than at the end of fixation (LATE), whereas the low-gamma power showed the opposite tendency: stronger at the end of fixation (LATE) than at the beginning of fixation (EARLY). Figure 4*D* presents a detailed temporal comparison of the power changes in high gamma, low gamma, and the theta phase shift of spike timing.

*Theta phase-based modulation of gamma-band oscillation.* To examine the relationship between the theta and gamma oscillations during fixation, we computed a time-frequency plot, locked to the theta trough (Fig. 5*A*; the baseline theta was filtered from 6 to 10 Hz). In the time-frequency plot in the *left* panel of Fig. 5*A*, the gamma data were realigned to the theta trough nearest to fixation onset ($t = 0$) and averaged across all successful fixation trials ($n = 1{,}181$). In the *right* panel of Fig. 5*A*, the gamma data were realigned to the theta trough nearest to the offset of the fixation cue ($t = 1$). Again we observed a trend such that the high-gamma oscillations were stronger at the beginning of fixation and decreased across the fixation period, whereas the low-gamma oscillations became more prominent later in the fixation period (with the strongest low-gamma power around the middle of fixation). The low-gamma oscillations immediately decayed after the offset of the fixation cue, at which time the high-gamma oscillations suddenly reappeared. Another interesting feature was that the dynamics of the gamma power were modulated by the ongoing theta cycle. The high-gamma component was strong around the positive peak of the theta cycle, whereas the low-gamma component was strong around the negative trough of the theta cycle, similar to observations in several previous studies (Belluscio et al. 2012; Scheffer-Teixeira et al. 2012).

In Fig. 5*B* we also plotted the average gamma on the basis of the theta phase (i.e., phase-frequency plot; the baseline theta was filtered from 7 to 9 Hz). This was done because, compared with the theta oscillation in moving rats, the theta oscillation during immobility has a relatively unstable instantaneous profile, in terms of both frequency and amplitude (e.g., with sudden slowing of the frequency, or a sudden change in amplitude for just one or a few theta cycles). The plot was aligned with the prior theta trough nearest to the fixation onset. Because the mean frequency of the theta in this figure was about 8 Hz, the fixation period roughly corresponded to the duration from 0 to the 8th theta cycle in this figure. Consistent with the previous figures, this plot also showed that the power

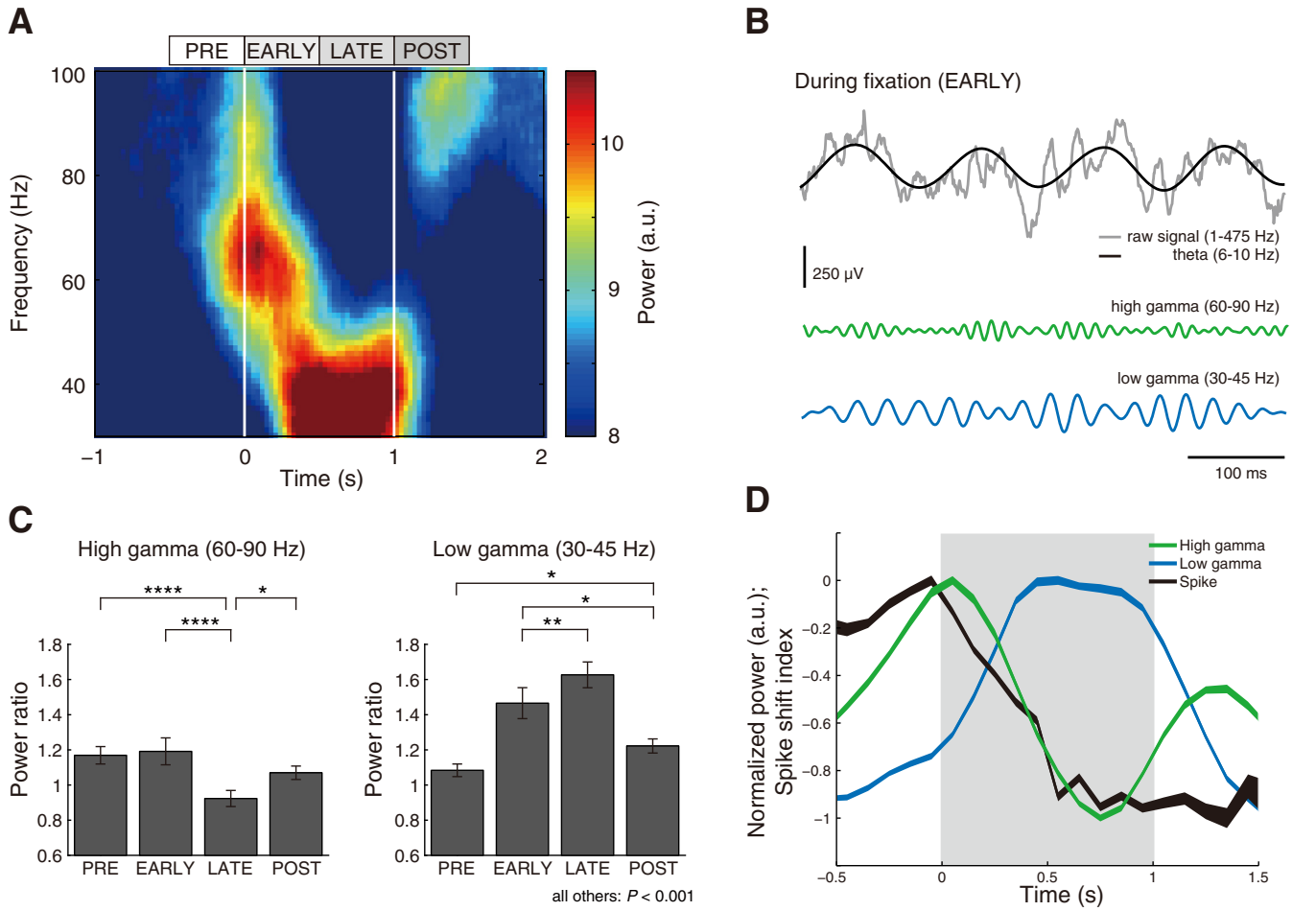


Fig. 4. The dynamics of hippocampal gamma oscillation during fixation. *A*: the power spectrogram (0.5-Hz steps, normalized by the total power in the time window from −1.5 to +2.5 s from fixation onset; $n$ = 1,181 trials). *B*: example LFP traces. The green and blue traces indicate the high- and low-gamma oscillations during the first half of the fixation period. The two gamma oscillations occur at different phases relative to the ongoing theta (black line; the gray line represents the raw LFP trace). *C*: normalized mean power ratios for high gamma and low gamma during four 0.5-s periods around fixation (normalized by the power from −2 to −1.5 s relative to fixation onset; *$P < 0.05$; **$P < 0.01$; ****$P < 0.001$; $n$ = 18 sessions, same as Fig. 1*E*). *D*: comparison of the spike phase shift with LFP dynamics during the fixation period ($n$ = 1,181 trials). The mean firing phase angle of the sequence-dependent fixation cells in the preferred sequence trials was computed for each 0.1-s bin and drawn in black. The mean LFP power dynamics for high and low gamma was normalized corresponding to 0 for the positive peak and −1 for the negative trough. The power of the corresponding range was estimated from the spectrogram and normalized in the range of −1 to 0 for the minimum and maximum values within the analyzed period (−0.5 to +1.5 s from the fixation onset). Colored bands for each line indicate SEM. Three observations emerge: the peak of low-gamma power precedes the trough (negative peak) of the high-gamma power; the shift in spike timing appears more irregular, starting earlier than the decrease of high-gamma power, but showing a shallower slope; the LFP power started to recover after the fixation period, whereas the shift in spike timing did not.

of high-gamma oscillation decreased toward the end of fixation, whereas the low-gamma component gradually appeared a few theta cycles after the fixation onset. This low-gamma component disappeared soon after the end of fixation, at which time the high-gamma component reappeared. The high-gamma component was phase-locked to the positive peak, whereas the low-gamma component was phase-locked to the negative trough of the ongoing theta cycle.

To elucidate this relationship between the gamma power and the theta phase angle, we constructed a histogram showing the number of peaks of high- or low-gamma oscillations in each theta phase (Fig. 5*C*). Each peak of gamma oscillation was detected by searching the peak of the envelope (computed by Hilbert transform) of the filtered LFP signal (60–90 Hz for high gamma and 30–45 Hz for low gamma). This was done each time within (non-overlapping) pairs of two consecutive theta cycles to prevent counting small peaks (following a procedure similar to that of Tort et al. 2008). The bin width for these histograms was 18°. The results confirmed that the high-gamma oscillation was anchored around the positive peak of the theta cycle, whereas the low-gamma oscillation was anchored around the negative trough.

To quantify the phase-amplitude cross-frequency coupling, we computed the Modulation Index (Tort et al. 2010) for the data of within two theta cycles from the theta trough nearest to the fixation onset and nearest to the middle of the fixation ($t$ = 0.5 s); that is, for the period of, respectively, the most prominent high- and low-gamma power (see Fig. 5, *D* and *E*). The distribution of Modulation Index values suggested that this modulation was strong for the theta band range (6–10 Hz) for both high and low gamma. Although both high and low gamma were significantly modulated by the theta rhythm around both fixation onset and the middle of fixation, the Modulation Index values suggested that, for both high and low gamma, the

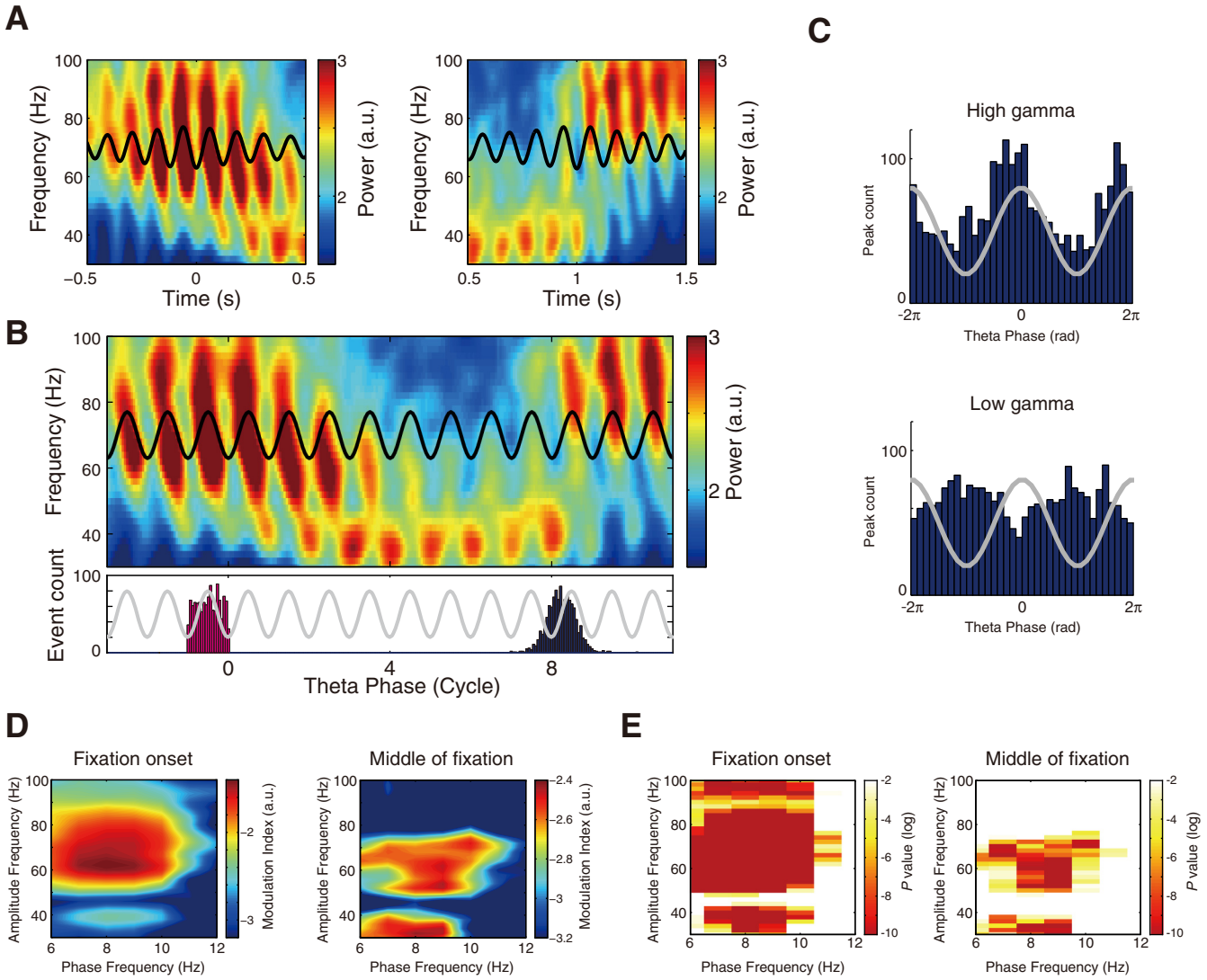


Fig. 5. The dynamics of the theta phase modulation of hippocampal gamma oscillations. *A*: time-frequency plots of the mean normalized power, aligned to the theta trough nearest to the fixation onset (*left* panel; $t = 0$) and the fixation cue offset (*right* panel; $t = 1$) ($n = 1{,}181$ trials). The theta trough-aligned averaged LFP signal (band-pass filtered, 6–10 Hz) is shown in black in both panels. *B*: frequency plot of the mean normalized power for the theta phase vs. gamma band, aligned to the prior theta trough nearest to the fixation onset. The theta phase trace is shown in black in the plot. The distribution of the actual timings of the fixation onset (magenta) and the fixation cue offset (blue) are shown in histograms below the plot. *C*: the histograms of the theta phases at which the peaks of the high- (60–90 Hz) and low-gamma (30–45 Hz) oscillations occurred during the fixation period. The theta phase trace is shown in gray. *D*: phase-to-amplitude co-modulograms showing theta modulation of gamma oscillation on a logarithmic scale ($n = 1{,}181$ trials). The *left* panel shows the results obtained from the gamma-band data within two theta cycles from the theta trough nearest to the fixation onset. The *right* panel shows the results obtained for the theta trough nearest to the middle of fixation. We used different color scales in the plots for fixation onset and the middle of fixation to optimize the visibility of components. *E*: statistical significance of the phase-to-amplitude co-modulograms were tested by the surrogate method (see MATERIALS AND METHODS). The colored area (bin size: 1 Hz for *x*-axis and 2 Hz for *y*-axis) indicates the level of statistical significance (*P* value) using a log scale. The area with *P* value $< 0.01$ is shown in white.

strength of coupling with theta oscillation was most prominent around the onset of fixation and decreased in the middle of fixation.

*Neural activity in error trials with premature fixation break.* The average number of erroneous-fixation trials per session was 51.4 (SD 14.8). The distribution of error fixation times (i.e., the time of erroneous-fixation break) was examined with a total of 926 erroneous-fixation trials. We tested the theta phase shift in spike timing (of the sequence-dependent fixation cells; $n = 24$) during erroneous fixation. Because there were trials during which multiple fixation cells could be recorded, the database amounted to 1,596 trials in total. We divided the trials into three subgroups with respect to the fixation time: short latency (0–0.33 s; $n = 121$), medium latency (0.34–0.66 s; $n = 155$), and long latency (0.67–1 s; $n = 1{,}320$). Figure 6 presents the phase-to-time color plots of the population trends for the neurons' preferred trial sequences (panel *A*) and non-preferred trial sequences (panel *B*). For the preferred sequence, the theta phase shift in spike timing can be seen in the long-latency trials (*right*-most panel), starting from the positive peak (0°) toward the negative trough (−180°), similar to the data in correct trials (see Fig. 2). There is also a hint of a shift in the medium-latency trials (*middle* panel), but not in the short-latency trials (*left* panel). For the nonpreferred sequence, there were no clear tendencies, as was the case also in correct trials (Fig. 2; for statistical analysis, see Fig. 6*C*).

We also drew the normalized power spectrograms for these three types of error trials in Fig. 7 (following the same procedures as for Fig. 3*A*). High-gamma oscillation became more obvious and stabilized around fixation onset in the longer latency trials, whereas the low-gamma components were more prominent around the fixation break. In short, the spectrogram profile progressively looked more similar to that of correct trials with longer fixation durations before a premature break:

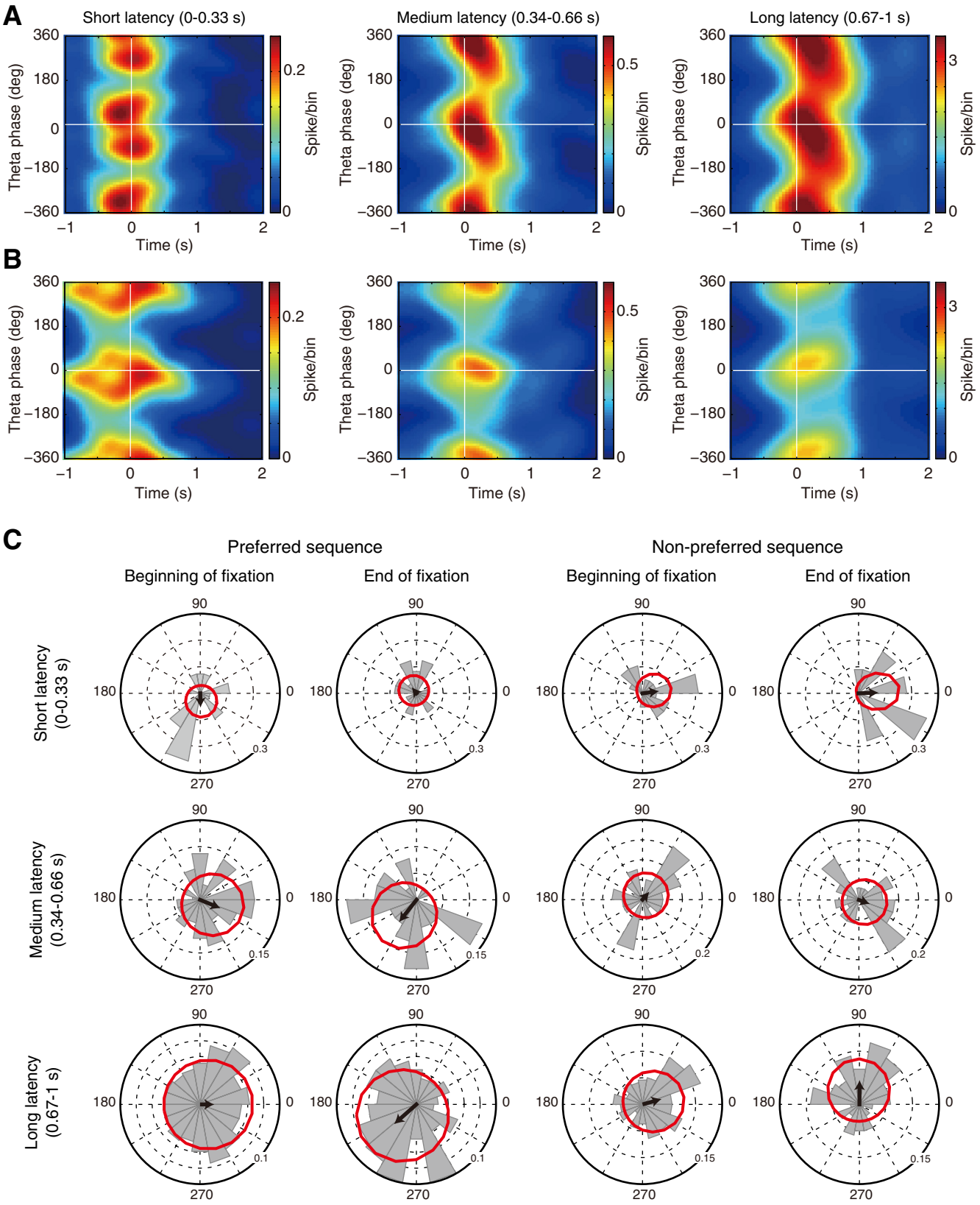

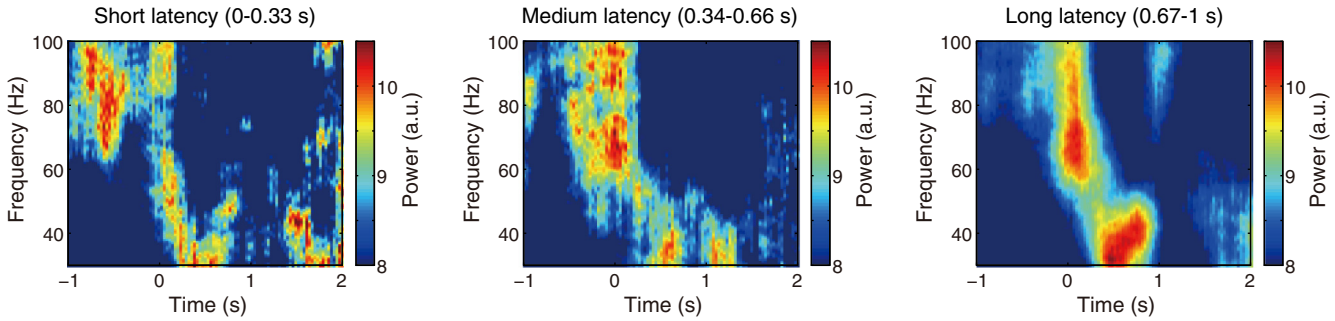


Fig. 7. The LFP dynamics in error trials (when the rat made a premature fixation break). The three normalized LFP spectrograms correspond to the population data obtained from short-latency erroneous-fixation trials (with a fixation duration of 0–0.33 s; $n = 75$ trials), medium-latency erroneous-fixation trials (0.34–0.66 s; $n = 96$ trials), and long-latency erroneous-fixation trials (0.67–1 s; $n = 755$ trials); format is the same as in Fig. 4*A*.

the longer the fixation duration, the more similarity with the activity in correct trials.

## DISCUSSION

One of the key approaches to studying brain function is to examine time-locked signals to specific external events and internal brain rhythms, under tightly controlled physical conditions. However, to date, no study has achieved this in memory-related behavioral processes with rodents due to difficulties in task design. Our laboratory recently developed a new paradigm with a 1-s fixation (sustained nose-poking) that provides exact enter and leave events during a memory-guided spatial alternation task (Takahashi et al. 2009a, 2009b). These enter and leave events clearly demarcate a fixation period, a period during which the rat can only rely on memory. During this period, the rat has no access to motor or sensory cues from which to derive a code for spatial alternation. Thus any alternation coding during this period should reflect mnemonic coding, whereas, at other moments in the trial, it is more difficult to disentangle motor, sensory and mnemonic activity. This task allows us to capture the moment-by-moment changes in the hippocampal signals and align these temporally on a trial-by-trial basis relative to the fixation period.

Using this task, we observed neural mechanisms that code spatial alternation in hippocampal CA1 during the 1-s fixation, not only in the firing rate (Takahashi et al. 2009a, 2009b), but also in the dynamics of spike timing and gamma oscillation. These dynamics were anchored to the ongoing theta oscillation. First, the spike timing of CA1 pyramidal neurons shifted from the positive theta peaks at the beginning of fixation to the negative troughs at the end of fixation (Fig. 2). Second, the gamma-band oscillation showed remarkable changes as well, with strong high-gamma power particularly at the positive theta peaks during the beginning of fixation, followed by a reduction later during fixation; conversely, there was an increase of low-gamma power later on in the fixation period, phase-locked to the negative troughs of theta (Fig. 5). The analysis of the error trials with premature fixation breaks indicated that the changes in spiking and gamma oscillations correlated with the timing of the nose-poke release (Figs. 6 and 7).

*Theta-based shift in spike timing during fixation.* Our finding of a shift in spike timing relative to theta is reminiscent of theta phase precession (O'Keefe and Recce 1993; Skaggs et al. 1996), but clearly deviates from the classic concept. A striking difference with previous reports about theta phase precession during actual or virtual running is that the phase shift we observed shows sequence dependency: it occurred only in the preferred sequences. Such preferences for LEFT-TO-RIGHT vs. RIGHT-TO-LEFT trials emerge at the single neuron level, and cannot be observed in the LFP signal pattern. In this sense, the spike phase shift in preferred-sequence trials also reflects a type of selectivity that does not apply to the gamma changes during fixation, which are observed across all trials. It suggests that CA1 neurons do not passively reflect, but selectively process the gamma inputs.

Several researchers have reported theta phase precession while the subject stays at the same location (e.g., while running in a wheel; Harris et al. 2002; Pastalkova et al. 2008), suggesting that changes of sensory (visual) input are not required for theta phase precession. However, our data of a shift in spike timing, obtained while the rat was sitting and waiting, suggest that theta phase precession can occur during awake behaviors, reflecting purely internally generated neural dynamics, unaffected by sensory or motor changes. Precession-like activity has also been observed during random eye movement sleep (Harris et al. 2002), under a theta rhythm analogous to that of

Fig. 6. *A*: spike timing relative to the theta phase in error trials (when the rat made a premature fixation break). The erroneous-fixation trials are divided in three latency groups as a function of the duration of fixation until premature fixation break: short-latency erroneous-fixation trials (0–0.33 s), medium-latency erroneous-fixation trials (0.34–0.66 s), and long-latency erroneous-fixation trials (0.67–1 s). The population graphs for the spike timing relative to theta in erroneous-fixation trials are shown in the same format as Fig. 2*A*. The panels represent the population data for the three latency groups in the preferred-sequence trials. *B*: the data in the nonpreferred-sequence trials. *C*: the angle histogram plots from the data obtained 150 ms after the fixation onset and 150 ms before the fixation break in the erroneous-fixation trials. The properties are shown separately for the preferred vs. nonpreferred sequence in the short-, medium-, and long-latency erroneous fixation trials, in the same format as that of Fig. 2*D*. To examine these phase-shift trends statistically, we tested the bias in spike phase angle from 0 to 0.15 s after the fixation onset and for the last 0.15 s before the premature fixation break for each of three groups and performed V tests for nonuniformity of circular data with a specified mean direction. For the preferred-sequence trials, the spike data around fixation onset showed a significant bias to the positive peak (0°) of the theta cycle in the medium-latency ($P < 0.01$; $n = 68$ spikes) and the long-latency ($P < 0.01$; $n = 401$ spikes) trials, but not such a significant bias in the short-latency ($n = 27$ spikes). Around offset of the premature fixations, the spike timings were biased to the negative trough (180°) of the theta cycle in the medium-latency ($P < 0.05$; $n = 38$ spikes) and long-latency ($P < 0.005$; $n = 181$ spikes) trials, but again no significant bias in the short-latency trials ($n = 24$ spikes). No such trend was seen for the nonpreferred sequence in all of these three types of trials.

mobile periods. Poe et al. (2000) observed shifts from peak to trough during rapid eye movement sleep, analogous to the sudden changes seen in our data; however, the shifts they observed occurred across days and depended on changes from novelty to familiarity. The shifts we observed occurred during awake, attentive behaviors. Following the characterization of different theta oscillations (e.g., Bland 2009; Kramis et al. 1975), this result implies that the present shift in spike timing likely occurred under type 2 theta (observed when the rat is immobile, but alert).

We also noted that, in our paradigm, the phase shift during fixation moved from the positive peak in the ongoing theta cycle to the negative trough, a phase difference of 180° rather than the 360° cycles seen in the prototypical phase precession with rats moving through place fields. Computational studies have suggested that the theta phase precession consists of two separable components, possibly dependent on different neural mechanisms (Yamaguchi et al. 2002, 2007). Other work has suggested that, in a single trial, the theta phase precession advances only 180°, whereas the onset of the precession varies widely so that the population average gives the impression of 360° precession (Schmidt et al. 2009). Both ideas are compatible with our data, suggesting a shift of one-half a cycle in a tightly controlled behavioral paradigm, producing limited variability in the onset of the shift.

Although at the population level (Figs. 2*B* and 3*A*) the shift of spike timing in preferred-sequence trials appeared gradual and linear, reminiscent of theta phase precession, a different picture emerged when examining the spiking phase shift on a trial-by-trial basis (Fig. 3, *B* and *C*). We found striking variability in the type of shift, with the majority of individual trials producing poor linearity fits and slopes that differed from that of the population. In some trials, the shift appeared quite sudden; in other trials the shift went through an unstable, noisy phase before settling on the negative trough. Overall, the shift suggests a transition between states, not a smooth precession.

*Flow of information in hippocampus during fixation.* Using our paradigm, we also obtained a surprising and marked change in gamma processing from high to low gamma during the fixation period. No one has so far been able to relate gamma differences to behavioral processing, although several researchers have suggested that gamma frequencies may indicate the functional connectivity and information processing (e.g., Canolty et al. 2006; Colgin et al. 2009; Lisman 2005). Using our new task, we found that each gamma component is strongly phase-locked to a specific theta phase, and that these power changes in each band occur abruptly a few theta cycles after the fixation onset.

In this respect, our data provide an informative contrast with previous studies that have highlighted the role of running speed in the frequency of the gamma oscillation (Ahmed and Mehta 2012; Chen et al. 2011; Kemere et al. 2013). Here, the systematic variation in theta-based gamma oscillation was observed while the rats were not moving. The analysis of the erroneous fixation trials further indicated that this systematic gamma variation correlated with the timing of action initiation after fixation. Thus the systematic gamma variation appears to be an important aspect of spatial-alternation coding in hippocampus under the present behavioral paradigm.

Interestingly, the gamma variation appeared to reflect separable dynamics for high gamma and low gamma. The temporal profile of the reduction in high-gamma power through the fixation period started to reduce at around 100 ms after fixation onset and reached minimal power at around 800 ms after fixation onset. However, the temporal profile of the low-gamma power did not appear to be the inverse or mirror image of these dynamics. In contrast, the power increase of low gamma started even before fixation onset and reached maximal power at around 500 ms after fixation onset (see Fig. 4*D*).

Here, we can build on previous work to estimate the flow of information in hippocampus, following well-established proposals that high gamma (60–90 Hz) derives from outside the hippocampus (i.e., entorhinal cortex), whereas low gamma (30–45 Hz) originates from intra-hippocampal circuitry (i.e., CA3-CA1 network) (Bragin et al. 1995; Colgin et al. 2009; Csicsvari et al. 2003; see Fig. 8). Our findings with dominant high gamma at the very beginning of the fixation period, phase-locking to the positive theta peak, suggest an early role for entorhinal input. On the other hand, low gamma gradually increased in power, phase-locking to the negative theta trough, suggesting an important role for CA3 as the fixation period progressed. This proposal for the information flow may also accommodate the classic distinction of two types of theta: type 1 theta in CA1, which is dominant during active exploration, is thought to be derived from EC, whereas type 2 theta, which relates to immobility and attention, reaches CA1 via CA3

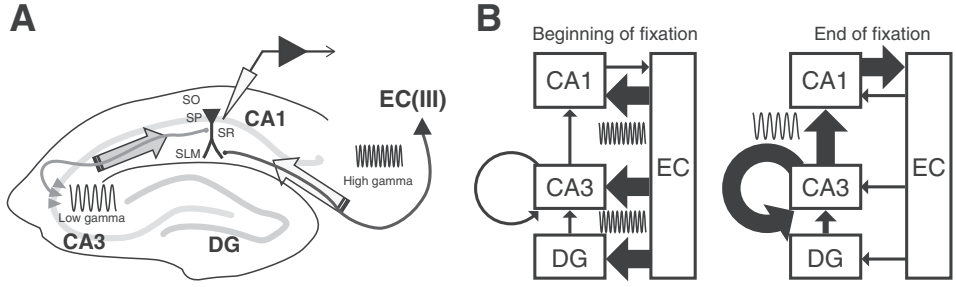


Fig. 8. Schematic presentation of the proposed information flow during fixation in hippocampus. *A*: CA1 receives two major input streams: one from entorhinal cortex (EC) layer III with high-gamma oscillation to the distal part of CA1 (stratum lacunosum-moleculare: SLM); the other from CA3 with low-gamma oscillation to the proximal part of CA1 (stratum radiatum; SR and stratum oriens; SO). The recordings in the current study were taken from the pyramidal cell layer of CA1 (stratum pyramidale; SP). DG, dentate gyrus. *B*: the hypothesized information flow during fixation. *Left*: at the beginning of fixation, strong external input is provided via EC, with high-gamma oscillation, to all of the hippocampal subregions. This signal would elicit further processing by the hippocampal circuit. The synaptic signals from CA3 at this time are weak, preventing confusion with representations from memory. *Right*: at the end of fixation, the input from EC weakens, but that from CA3, with slow gamma oscillation, gains in strength. This facilitates the retrieval of task-relevant representations from memory, without interference from other information.

(Bland 2009). The phase-amplitude coupling analysis in our study suggested that the high- and low-gamma frequencies are coupled to distinct phases in the theta-band oscillation (Fig. 5, *B* and *C*). Further studies using pharmacological and genetic tools are essential to elucidate the precise nature of the mapping between different types of gamma and theta in hippocampus.

We hypothesize that CA1 receives input from entorhinal cortex at the beginning of fixation, providing information about the current context (including sensory and motor parameters; perhaps mainly the onset of the fixation cue). This signal would elicit further, auto-associative intrahippocampal processing via CA3 to recall the required action, or to look up in memory the appropriate task sequence given the current context. This cognitive mechanism, then, would produce the discrimination of preferred and nonpreferred sequences in the average spike count and would determine the firing phase with respect to the ongoing theta rhythm.

This hypothetical view can be further elaborated in line with the proposals by Hasselmo (2005), suggesting that the hippocampus has two functional modes for each side of the theta cycle: encoding at the positive peak of the CA1 cell layer theta, and retrieval at the negative trough (see also Brankack et al. 1993; Hasselmo et al. 2002; Hyman et al. 2003). In this model, at the beginning of fixation, the hippocampus would be in the encoding mode, receiving strong input from entorhinal cortex; then, as the fixation period progresses, the hippocampus would switch to the retrieval mode, in which CA1 receives strong input from CA3 through Schaffer collaterals.

## ACKNOWLEDGMENTS

We thank M. Tsukada, Y. Sakurai, and Y. Isomura for advice and comments on the research.

## GRANTS

This work was supported by Human Frontier Science Program award RGP0039/2010; Grant-in-Aid for Scientific Research on Innovative Areas "Neural creativity for communication" (24120710); "Comprehensive Brain Science Network"; Tamagawa Global Center of Excellence Program of The Ministry of Education, Culture, Sports, Science, and Technology, Japan; and the Narishige Neuroscience Research Foundation. H. Nishida is a Research Fellow of Japan Society for the Promotion of Science.

## DISCLOSURES

No conflicts of interest, financial or otherwise, are declared by the author(s).

## AUTHOR CONTRIBUTIONS

Author contributions: M.T., A.D.R., and J.L. conception and design of research; M.T. performed experiments; M.T., H.N., A.D.R., and J.L. analyzed data; M.T., H.N., A.D.R., and J.L. interpreted results of experiments; M.T., H.N., A.D.R., and J.L. prepared figures; M.T. and J.L. drafted manuscript; M.T., H.N., A.D.R., and J.L. edited and revised manuscript; M.T., H.N., A.D.R., and J.L. approved final version of manuscript.

## REFERENCES

**Ahmed OJ, Mehta MR.** Running speed alters the frequency of hippocampal gamma oscillations. *J Neurosci* 32: 7373–7383, 2012.

**Belluscio MA, Mizuseki K, Schmidt R, Kempter R, Buzáki G.** Cross-frequency phase-phase coupling between theta and gamma oscillations in the hippocampus. *J Neurosci* 32: 423–435, 2012.

**Bland BH.** Anatomical, physiological, and pharmacological properties underlying hippocampal sensorimotor integration. In: *Information Processing by Neuronal Populations*, edited by Hölscher C, Munk M. New York: Cambridge University Press, 2009, p. 283–325.

**Bland BH, Oddie SD.** Theta band oscillation and synchrony in the hippocampal formation and associated structures: the case for its role in sensorimotor integration. *Behav Brain Res* 127: 119–136, 2001.

**Bokil H, Andrews P, Kulkarni JE, Mehta S, Mitra PP.** Chronux: a platform for analyzing neural signals. *J Neurosci Methods* 192: 146–151, 2010.

**Bower MR, Euston DR, McNaughton BL.** Sequential-context-dependent hippocampal activity is not necessary to learn sequences with repeated elements. *J Neurosci* 25: 1313–1323, 2005.

**Bragin A, Jandó G, Nádasdy Z, Hetke J, Wise K, Buzsáki G.** Gamma (40–100 Hz) oscillation in the hippocampus of the behaving rat. *J Neurosci* 15: 47–60, 1995.

**Brankack J, Stewart M, Fox SE.** Current source density analysis of the hippocampal theta rhythm: associated sustained potentials and candidate synaptic generators. *Brain Res* 615: 310–327, 1993.

**Buzsáki G.** *Rhythms of the Brain*. New York: Oxford University Press, 2006.

**Canolty RT, Edwards E, Dalal SS, Soltani M, Nagarajan SS, Kirsch HE, Berger MS, Barbaro NM, Knight RT.** High gamma power is phase-locked to theta oscillations in human neocortex. *Science* 313: 1626–1628, 2006.

**Carr MF, Karlsson MP, Frank LM.** Transient slow gamma synchrony underlies hippocampal memory replay. *Neuron* 75: 700–713, 2012.

**Chen Z, Resnik E, McFarland JM, Sakmann B, Mehta MR.** Speed controls the amplitude and timing of the hippocampal gamma rhythm. *PLos One* 6: e21408, 2011.

**Colgin LL, Denninger T, Fyhn M, Hafting T, Bonnevie T, Jensen O, Moser MB, Moser EI.** Frequency of gamma oscillations routes flow of information in the hippocampus. *Nature* 462: 353–357, 2009.

**Csicsvari J, Hirase H, Czurkó A, Mamiya A, Buzsáki G.** Oscillatory coupling of hippocampal pyramidal cells and interneurons in the behaving rat. *J Neurosci* 19: 274–287, 1999.

**Csicsvari J, Jamieson B, Wise KD, Buzsáki G.** Mechanisms of gamma oscillations in the hippocampus of the behaving rat. *Neuron* 37: 311–322, 2003.

**Davidson TJ, Kloosterman F, Wilson MA.** Hippocampal replay of extended experience. *Neuron* 63: 497–507, 2010.

**Diba K, Buzsáki G.** Forward and reverse hippocampal place-cell sequences during ripples. *Nat Neurosci* 10: 1241–1242, 2007.

**Ferbinteanu J, Shapiro ML.** Prospective and retrospective memory coding in the hippocampus. *Neuron* 40: 1227–1239, 2003.

**Foster DJ, Wilson MA.** Reverse replay of behavioural sequences in hippocampal place cells during awake state. *Nature* 440: 680–683, 2006.

**Gupta AS, van der Meer MA, Touretzky DS, Redish AD.** Hippocampal replay is not a simple function of experience. *Neuron* 65: 695–705, 2010.

**Gupta AS, Van der Meer MA, Touretzky DS, Redish AD.** Segmentation of spatial experience by hippocampal theta sequences. *Nat Neurosci* 15: 1032–1039, 2012.

**Harris KD, Henze DA, Hirase H, Leinekugel X, Dragoi G, Czurkó A, Buzsáki G.** Spike train dynamics predicts theta-related phase precession in hippocampal pyramidal cells. *Nature* 417: 738–741, 2002.

**Harvey CD, Collman F, Dombeck DA, Tank DW.** Intracellular dynamics of hippocampal place cells during virtual navigation. *Nature* 461: 941–946, 2009.

**Hasselmo ME.** What is the function of hippocampal theta rhythm? Linking behavioral data to phasic properties of field potential and unit recording data. *Hippocampus* 15: 936–949, 2005.

**Hasselmo ME, Bodelón C, Wyble BP.** A proposed function for hippocampal theta rhythm: separate phases of encoding and retrieval enhance reversal of prior learning. *Neural Comput* 14: 793–817, 2002.

**Hyman JM, Wyble BP, Goyal V, Rossi CA, Hasselmo ME.** Stimulation in hippocampal region CA1 in behaving rats yields long-term potentiation when delivered to the peak of theta and long-term depression when delivered to the trough. *J Neurosci* 23: 11725–11731, 2003.

**Jezek K, Henriksen EJ, Treves A, Moser EI, Moser MB.** Theta-paced flickering between place-cell maps in the hippocampus. *Nature* 478: 246–249, 2011.

**Johnson A, Redish AD.** Neural ensembles in CA3 transiently encode paths forward of the animal at a decision point. *J Neurosci* 27: 12176–12189, 2007.

**Karlsson MP, Frank LM.** Awake replay of remote experiences in the hippocampus. *Nat Neurosci* 12: 913–918, 2009.

**Kemere C, Carr MF, Karlsson MP, Frank LM.** Rapid and continuous modulation of hippocampal network state during exploration of new place. *PLos One* 8: e73114, 2013.

**Kempter R, Leibold C, Buzsáki G, Diba K, Schmidt R.** Quantifying circular-linear associations: hippocampal phase precession. *J Neurosci Methods* 207: 113–124, 2012.

**Kramis R, Vanderwolf CH, Bland BH.** Two types of hippocampal rhythmical slow activity in both the rabbit and the rat: relations to behavior and effects of atropine, diethyl ether, urethane, and pentobarbital. *Exp Neurol* 49: 58–85, 1975.

**Lever C, Wills T, Cacucci F, Burgess N, O'Keefe J.** Long-term plasticity in hippocampal place-cell representation of environmental geometry. *Nature* 416: 90–94, 2002.

**Lisman J.** The theta/gamma discrete phase code occurring during the hippocampal phase precession may be a more general brain coding scheme. *Hippocampus* 15: 913–922, 2005.

**Lisman J, Redish AD.** Prediction, sequences and the hippocampus. *Philos Trans R Soc Lond B Biol Sci* 364: 1193–1201, 2009.

**Mitra P, Bokil H.** *Observed Brain Dynamics*. New York: Oxford University Press, 2008.

**O'Keefe J, Nadel L.** *The Hippocampus as a Cognitive Map*. Oxford, UK: Clarendon, 1978.

**O'Keefe J, Recce ML.** Phase relationship between hippocampal place units and the EEG theta rhythm. *Hippocampus* 3: 317–30, 1993.

**O'Neil J, Senior TJ, Allen K, Huxter JR, Csicsvari J.** Reactivation of experience-dependent cell assembly patterns in the hippocampus. *Nat Neurosci* 11: 209–215, 2008.

**Pastalkova E, Itskov V, Amarasingham A, Buzsáki G.** Internally generated cell assembly sequences in the rat hippocampus. *Science* 321: 1322–1327, 2008.

**Paxinos G, Watson C.** *The Rat Brain in Stereotaxic Coordinates* (5th Ed.). San Diego, CA: Elsevier Academic, 2004.

**Poe GR, Nitz DA, McNaughton BL, Barnes CA.** Experience-dependent phase-reversal of hippocampal neuron firing during REM sleep. *Brain Res* 855: 176–180, 2000.

**Redish AD.** *Beyond the Cognitive Map: From Place Cells to Episodic Memory*. Cambridge, MA: MIT, 1999.

**Royer S, Zemelman BV, Losonczy A, Kim J, Chance F, Magee JC, Buzsáki G.** Control of timing, rate and bursts of hippocampal place cells by dendritic and somatic inhibition. *Nat Neurosci* 15: 769–775, 2012.

**Sakurai Y.** Involvement of auditory cortical and hippocampal neurons in auditory working memory and reference memory in the rat. *J Neurosci* 14: 2606–2623, 1994.

**Sakurai Y.** Hippocampal and neocortical cell assemblies encode memory processes for different types of stimuli in the rat. *J Neurosci* 16: 2809–2819, 1996.

**Scheffer-Teixeira R, Beichior H, Caixeta FV, Souza BC, Ribeiro S, Tort AB.** Theta phase modulates multiple layer-specific oscillations in the CA1 region. *Cereb Cortex* 22: 2404–2414, 2012.

**Schmidt R, Diba K, Leibold C, Schmitz D, Buzsáki G, Kempter R.** Single-trial phase precession in the hippocampus. *J Neurosci* 29: 13232–13241, 2009.

**Schmitzer-Torbert N, Redish AD.** Neuronal activity in the rodent dorsal striatum in sequential navigation: separation of spatial and reward responses on the multiple T task. *J Neurophysiol* 91: 2259–2272, 2004.

**Skaggs WE, McNaughton BL, Wilson MA, Barnes CA.** Theta phase precession in hippocampal neuronal populations and the compression of temporal sequences. *Hippocampus* 6: 149–172, 1996.

**Smith DM, Mizumori SJ.** Learning-related development of context-specific neuronal responses to places and events: the hippocampal role in context processing. *J Neurosci* 26: 3154–3163, 2006.

**Takahashi M, Lauwereyns J, Sakurai Y, Tsukada M.** A code for spatial alternation during fixation in rat hippocampal CA1 neurons. *J Neurophysiol* 102: 556–567, 2009a.

**Takahashi M, Lauwereyns J, Sakurai Y, Tsukada M.** Behavioral state-dependent episodic representations in rat CA1 neuronal activity during spatial alternation. *Cogn Neurodyn* 3: 165–175, 2009b.

**Tort AB, Kramer MA, Thorn C, Gibson DJ, Kubota Y, Graybiel AM, Kopell NJ.** Dynamic cross-frequency couplings of local field potential oscillations in rat striatum and hippocampus during performance of a T-maze task. *Proc Natl Acad Sci U S A* 105: 20517–20522, 2008.

**Tort AB, Komorowski RW, Manns JR, Kopell NJ, Eichenbaum H.** Theta-gamma coupling increases during the learning of item-context associations. *Proc Natl Acad Sci U S A* 106: 20942–20947, 2009.

**Tort AB, Komorowski R, Eichenbaum H, Kopell N.** Measuring phase-amplitude coupling between neuronal oscillations of different frequencies. *J Neurophysiol* 104: 1195–1210, 2010.

**Vanderwolf CH.** Limbic-diencephalic mechanisms of voluntary movement. *Psychol Rev* 78: 83–113, 1971.

**Wood ER, Dudchenko PA, Robitsek RJ, Eichenbaum H.** Hippocampal neurons encode information about different types of memory episodes occurring in the same location. *Neuron* 27: 623–633, 2000.

**Yamaguchi Y, Aota Y, McNaughton BL, Lipa P.** Bimodality of theta phase precession in hippocampal place cells in freely running rats. *J Neurophysiol* 87: 2629–2642, 2002.

**Yamaguchi Y, Sato N, Wagatsuma H, Wu Z, Molter C, Aota Y.** A unified view of theta-phase coding in the entorhinal-hippocampal system. *Curr Opin Neurobiol* 17: 197–204, 2007.

**Ylinen A, Bragin A, Nádasdy Z, Jandó G, Szabó I, Sik A, Buzsáki G.** Sharp wave-associated high-frequency oscillation (200 Hz) in the intact hippocampus: network and intracellular mechanisms. *J Neurosci* 15: 30–46, 1995.

**Zar JH.** *Biostatistical Analysis* (5th Ed.). Upper Saddle River, NJ: Prentice-Hall/Pearson, 2007.